Medical Image Analysis 14 (2010) 759–769

Contents lists available at ScienceDirect

Medical Image Analysis

journal homepage: www.elsevier.com/locate/media

Robust CTA lumen segmentation of the atherosclerotic carotid artery bifurcation in a large patient population

Rashindra Manniesing [a,*], Michiel Schaap [a], Sietske Rozie [b], Reinhard Hameeteman [a], Danijela Vukadinovic [a], Aad van der Lugt [b], Wiro Niessen [a,c]

[a] Biomedical Imaging Group Rotterdam, Departments of Medical Informatics and Radiology, Erasmus MC, Rotterdam, P.O. Box 2040, 3000 CA Rotterdam, The Netherlands
[b] Department of Radiology, Erasmus MC – University Medical Center Rotterdam, The Netherlands
[c] Imaging Science and Technology, Faculty of Applied Sciences, Delft University of Technology, The Netherlands

ARTICLE INFO

Article history:
Received 18 March 2009
Received in revised form 4 May 2010
Accepted 4 May 2010
Available online 1 June 2010

Keywords:
Lumen segmentation
Level set
CT angiography (CTA)
Atherosclerotic carotid bifurcation
Evaluation

ABSTRACT

We propose and validate a semi-automatic method for lumen segmentation of the carotid bifurcation in computed tomography angiography (CTA). First, the central vessel axis is obtained using path tracking between three user-defined points. Second, starting from this path, the segmentation is automatically obtained using a level set. The cost and speed functions for path tracking and segmentation make use of intensity and homogeneity slice-based image features. The method is validated on a large data set of 234 carotid bifurcations of 129 ischemic stroke patients with atherosclerotic disease. The results are compared to manually obtained lumen segmentations. Parameter optimization is carried out on a subset of 30 representative carotid bifurcations. With the optimized parameter settings the method successfully tracked the central vessel paths in 201 of the remaining 204 bifurcations (99%) which were not part of the training set. Comparison with manually drawn segmentations shows that the average overlap between the method and observers is similar (for the inter-observer set the results were 92% vs. 87% and for the intra-observer set 94% vs. 94%). Therefore the method has potential to replace the manual procedure of lumen segmentation of the atherosclerotic bifurcation in CTA.

1. Introduction

The carotid artery bifurcations are located laterally in the neck and are the major supplier of blood to the brain. Atherosclerosis is a vascular disease characterized by gradual accumulation of fatty material (i.e. plaque) inside the arteries, eventually leading to hardening of the plaque (calcium) and lumen narrowing (stenosis). A widely-used modality for diagnosis of the atherosclerotic carotid artery is computed tomography angiography (CTA) which provides detailed 3D information on the vessel lumen. Clinical, longitudinal and epidemiological studies on the atherosclerotic bifurcation, imaged using CTA, often require a robust lumen segmentation method.

Lumen segmentation of the carotid bifurcation facilitates subsequent analysis, including stenosis grading (Mildenberger et al., 1997; Scherl et al., 2007; Tarjàn et al., 1996) hemodynamic modeling (Antiga et al., 2002) and the detection and quantification of plaque components in the vessel wall (De Weert et al., 2008; Rozie et al., 2009; Vukadinovic et al., 2010). A variety of lumen segmentation methods are available ranging from simple region growing approaches to more advanced approaches like curve evolution (Lorigo et al., 2001; Zhuge et al., 2006; Yan and Kassim, 2006), particle filtering (Florin et al., 2005) and graph-cuts (Boykov and Jolly, 2001; Homann et al., 2008; Schaap et al., 2009). However, the value of these techniques for use in clinical practice is not yet established, since their evaluation is often limited to a relatively small and no-representative amount of patient data.

This study describes our method of lumen segmentation and demonstrates its ability to robustly and accurately segment the carotid bifurcation in a large population of patients with ischemic stroke. This population is representative for the anatomic and pathological diversity presented in clinical practice.

We propose a level set-based method that uses path tracking between user-defined points for initialization and for composing a speed function for the level set. Although similar two-step approaches have been reported (Aylward and Bullit, 2002; Van Bemmel et al., 2003a,b), besides implementation details, our work also

* Corresponding author. Tel.: +31 10 7043050; fax: +31 10 7044722.
E-mail addresses: r.manniesing@erasmusmc.nl (R. Manniesing), michiel.schaap@erasmusmc.nl (M. Schaap), s.rozie@erasmusmc.nl (S. Rozie), k.hameeteman@erasmusmc.nl (R. Hameeteman), d.vukadinovic@erasmusmc.nl (D. Vukadinovic), a.vanderlugt@erasmusmc.nl (A. van der Lugt), w.niessen@erasmusmc.nl (W. Niessen).

1361-8415/$ - see front matter © 2010 Elsevier B.V. All rights reserved.
doi:10.1016/j.media.2010.05.001

differs regarding the speed function. A properly designed speed function is essential for the final accuracy and robustness of level set-based segmentation approaches. The novelty of our speed function is that its intensity term is balanced between local and global statistics to control the level set evolution both at the coarse and fine level, and second, the inclusion of an intensity homogeneity term as a complementary driving force to distinguish vessel structures from non-vessel structures in the image.

This work is closely related to that of Scherl et al. (2007) and Van Bemmel et al. (2003b). Scherl and colleagues extend the Chan-and-Vese framework (Chan and Vese, 2001), i.e. active contours without edges, by including a third class to model background, lumen and higher intensity valued objects (such as bone and calcium) separately. In the Chan-and-Vese framework, the foreground and background classes are modeled by first-order statistics. Although this may be sufficient for modeling lumen intensity, it may not be the most appropriate approach for modeling background and the higher intensity valued objects in CTA. In the present study we impose a Gaussian distribution for the lumen intensities, and base the vessel boundary definition on this prior knowledge only. Furthermore, compared to Scherl et al. (2007) we do not update the sampled intensity statistics during evolution of the surface. Van Bemmel and colleagues (2003b) propose a similar level set-based method preceded by path tracking between user-defined points applied to magnetic resonance angiography (MRA) acquisitions of the carotid bifurcation. The main difference compared with ours, is that their method is particularly dedicated to MRA images, which is reflected in the different constructed cost and speed functions for path tracking and segmentation. Compared with both of these earlier studies, our method has been evaluated on a much larger patient population; to our knowledge, an evaluation of carotid CTA lumen segmentation on this large scale has not previously been reported.

2. Method

The potential of a level-set framework for vessel segmentation has been reported earlier, both in magnetic resonance imaging (MRI) (Lorigo et al., 2001; Van Bemmel et al., 2003a,b; Yan and Kassim, 2006) and CTA (Scherl et al., 2007; Zhuge et al., 2006). Of the various reasons for its wide-spread use, the most important are its ability to easily model complex geometries, to provide subvoxel accuracy in the resulting segmentation, and the possibility to steer the level set both with its geometrical properties and via the image-based speed terms. In the present study the geodesic active contour (GAC) framework (Caselles et al., 1997) is used as the basis of our segmentation method.

The method is initialized by clicking three points, i.e. in the common carotid artery and in the internal and external carotid artery (Fig. 1). Then, using a cost image and back propagation, paths through the internal and the external carotid artery are automatically extracted. These paths are subsequently used to construct an image-based speed function and to initialize the GAC. Each step is described in detail below.

2.1. Path tracking

In the present study, all patients have atherosclerotic disease in the carotid bifurcation giving rise to the presence of calcifications, soft plaque and/or lumen narrowing. To achieve a high degree of robustness, minimum user interaction is required by placing seed points in the common carotid artery and in the two branches of the bifurcation. In a fixed discrete and circular neighborhood around the seed points (see Section 5.1 for its exact value), an initial estimate is made of the statistics in the vessel by calculating the intensity mean μ and standard deviation σ. Two paths are then tracked, namely the internal and external carotid artery path, using the Dijkstra algorithm (Dijkstra, 1959) and voxel based backtracking. The essential element for path tracking is the definition of the cost function. In case of CTA, it is reasonable to assume that the intensity distribution of the contrast-enhanced vessel follows a Gaussian distribution, and we use the FWMH criterion[1] to construct the cost function. The FWHM criterion yields the lower and upper boundaries (the difference gives the width) of an arbitrary function at which the function reaches half of its maximum value. Given the intensity mean μ and intensity standard deviation σ and assuming a Gaussian distribution, the FWHM boundaries are described analytically by:

$$\beta_l = -\sigma\sqrt{2\ln 2} + \mu$$
$$\beta_u = +\sigma\sqrt{2\ln 2} + \mu$$

We map this distribution into a function which is equal to 1.0 at the mean vessel intensity and 0.5 at the FWHM criterion. This is achieved using two scaled and shifted error functions of which one is mirrored, as follows:

$$P_{fwhm} = \left(\frac{1}{2} + \frac{1}{2}erf\left(\frac{I-\beta_l}{\theta}\right)\right)\cdot\left(\frac{1}{2} - \frac{1}{2}erf\left(\frac{I-\beta_u}{\theta}\right)\right)$$

with $erf()$ the error function, I the image intensity and θ a user-defined slope of the error functions. An example of this function is shown in Fig. 2.

In addition, we observe that surrounding anatomical structures and imaging artifacts (such as streaking artifacts) have a more inhomogeneous intensity than the contrast vessels. A practical measure for inhomogeneity is the standard deviation of the intensity in a local circular neighborhood. Fig. 3 shows a typical example of this measure along the vessel. The difference between the global inhomogeneity and the per-slice inhomogeneity provides a good indication of regions containing severe streaking artifacts, and the difference between the per-slice inhomogeneity and the (non-)vessel inhomogeneity gives a good indication of the likelihood of a vessel. The standard deviation in a local discrete neighborhood (exact values are provided in Section 5) is thus a good representation of the inhomogeneity for that neighborhood. In the following we refer to this term as *noise,* to prevent possibly confusing use of the term 'standard deviation'. Let σ_g be the average noise of the complete data set, σ_s the average noise per slice and σ_v the vessel noise. Furthermore, let p_v be the likelihood of noise of an anatomical structure, i.e. the more homogeneous a structure is the closer p_v is to one, and let p_g be the likelihood of the noise of a slice. We then define the following additional function next to P_{fwhm} for path tracking:

$$P_{std} = p_v \cdot p_g + (1 - p_g)$$

as a slice based weighted probability function of the local noise in an image, with p_v and p_g using (positive) error functions, as follows:

[1] In MRA, a vessel boundary definition based on the FWHM criterion is usually associated with the following notion: find the maximum intensity value within the vessel lumen, and then the width of the vessel is the full width at half of this maximum value. This was introduced by Hoogeveen et al. (1998) and was determined according to phantom measurements in MRA and (amongst others) used for diameter measurements by Van Bemmel et al. (2003b). An important and reasonable underlying assumption is that for partial volume voxels half of its value is contributed by lumen and half by background. In the present study we model the lumen by imposing a Gaussian distribution on the lumen intensity statistics and subsequently define the lower and upper intensity thresholds based on the FWHM criterion applied to this distribution.

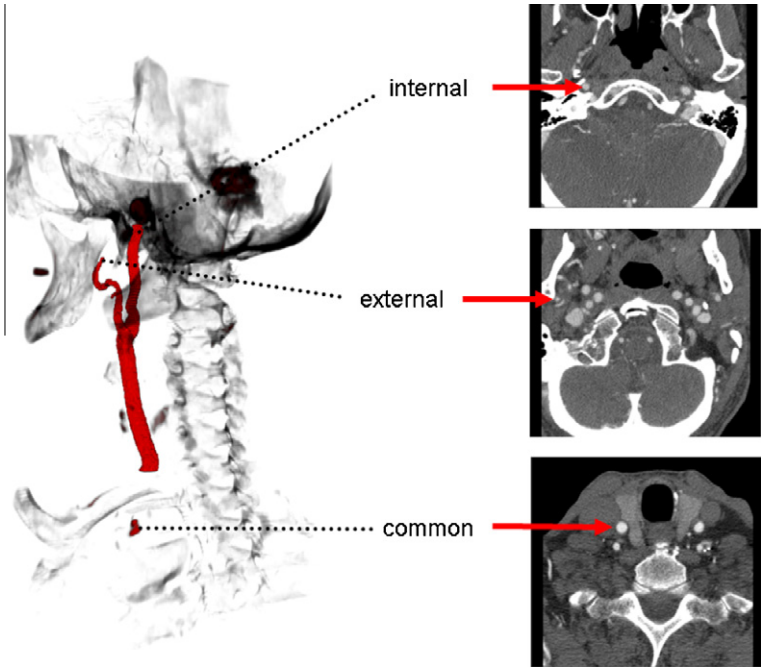

Fig. 1. The coverage of a typical CTA scan in patients with ischemic stroke is approximately from the aortic arch to midway the skull (volume rendering). Seed points for initialization of the method are placed in the common carotid artery (just above the aortic arch), the external carotid artery (near the skull) and the internal carotid artery (just below the skull base).

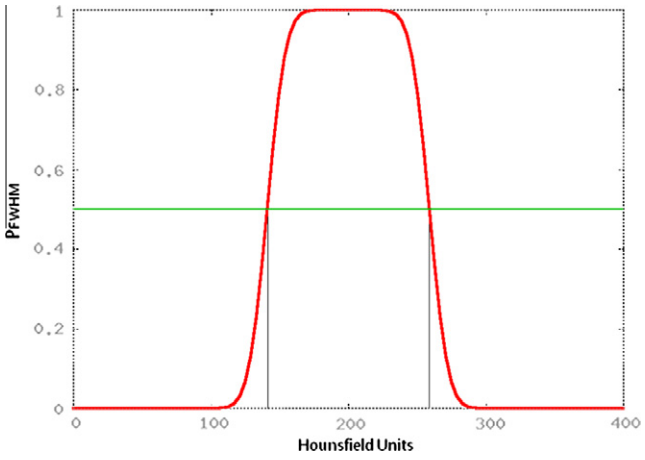

Fig. 2. Intensities within the vessel are assumed to follow a Gaussian distribution (not shown): we use its full width at half maximum (FWHM) criterion to construct a function for path tracking. This function is the result of two shifted and scaled error functions, such that at the mean vessel intensity its value is 1.0, and at the FWHM boundaries (denoted by the vertical lines in the graph) its value is 0.5.

$$p_v = \left(\frac{1}{2} + \frac{1}{2} erf\left(\frac{(\sigma_s - \sigma_v) - \alpha_v}{\theta_v}\right)\right)$$
$$p_g = 1 - \left(\frac{1}{2} + \frac{1}{2} erf\left(\frac{(\sigma_s - \sigma_g) - \alpha_g}{\theta_g}\right)\right)$$

with $\alpha_{v,g}$ thresholds of the standard deviation measures, and $\theta_{v,g}$ the slopes of the error functions. The slice based term p_g acts as a measure of reliability for the local term p_v. For example, in slices containing a lot of noise compared to the global noise level (e.g. as a result of streaking artifacts), p_g goes to zero letting P_{std} go to one (in which case image information is not taken into account and the path tracking algorithm will simply go in a straight line, i.e. straight perpendicular to the slices). On the other hand, if the slice does not contain a lot of noise compared to the global level, p_v becomes the dominant term and a local weighting is achieved by comparing the local noise σ_v with the slice noise σ_s.

The final likelihood function for path tracking P_{path} follows simply by:

$$P_{path} = P_{fwhm} P_{std}$$

of which both terms are normalized between [0, 1] before multiplication. P_{path} is then inverted to define the cost function, after addition of an epsilon value to prevent singularities, followed by the application of the Dijkstra algorithm starting at the point in the common carotid artery, properly weighting the cost function to account for possible voxel anisotropy. Finally, backtracking from the points in the internal and external arteries yields both paths.

2.2. GAC segmentation

We use the GACs approach for vascular lumen segmentation, which is described by the following partial differential equation

$$\Phi_t - \alpha \nabla F_{segm} \nabla \Phi + F_{segm}(1 - \gamma \kappa_{\min})|\nabla \Phi| = 0$$

with Φ the level set function, α the weighting of the advection term, F_{segm} the image-based speed term for segmentation, and γ the weighting of the minimal curvature term κ_{min}. Because vessels are tubular structures, κ_{max} is always large, and the smoothing term in level set-based segmentation is based on the minimal curvature only (Lorigo et al., 2001).

In a level set-based segmentation attention should be paid to the initialization, the image-based speed function and the stopping criterion. In our implementation, the level set is initialized based on the internal and external carotid artery paths extracted in the previous step. For this, a fast marching algorithm (Sethian, 1999) with fixed propagation speed is used to obtain the initial distance transform from a tube with radius ρ around the extracted paths.

The image-based speed function F_{segm} is defined by the image intensity and image gradient. If the gradient magnitude is greater than a threshold τ, the speed function is set to zero; otherwise, the speed is defined by the image intensity with a similar construction

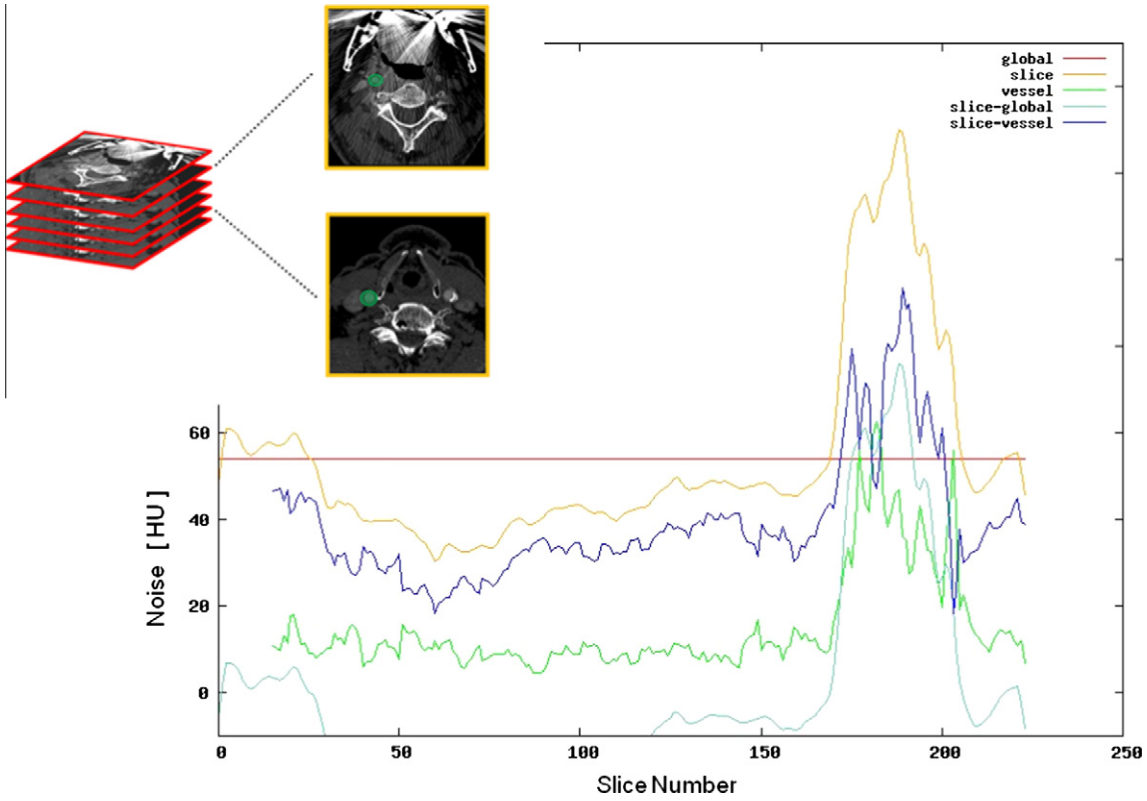

Fig. 3. An example of the noise level in the image as function of the axial position of one of the patient data of the training set for which a vessel lumen segmentation is available (see Section 5 for training of the method). The horizontal axes gives the axial position in the data set, the vertical axes the noise level as representative of the inhomogeneity in the image, which is calculated as the intensity standard deviation of every voxel with a fixed discrete and circular neighborhood. The average noise for the complete data set is given by the red line (3D volume), the average noise per slice is given by the yellow line (2D slice), the noise along a vessel path is given by the green line (see also green circle). The light and dark blue lines are the results of subtractions of the global and per-slice measure, and the per-slice and vessel measure. Based on this graph we can conclude that: (1) on average the inhomogeneity along the vessel is lower than along the slice, and (2) the inhomogeneity per slice dramatically increases at a specific region from approximately slice number 160 to 210. Inspection revealed the presence of streaking artifacts in that region.

of error functions as used for the intensity-based function for path tracking. We assume that the vessel intensities follow a Gaussian distribution, and construct F_{segm} such that for the mean vessel intensity the function goes to one, and at the FWHM boundaries β_l and β_u it goes to zero:

$$F_{segm} = \begin{cases} \left(-erf\left(\frac{I-\beta'_l}{\theta'}\right)\right) \cdot \left(erf\left(\frac{I-\beta'_u}{\theta'}\right)\right) & |\nabla I| < \tau \\ 0 & |\nabla I| \geqslant \tau \end{cases}$$

with $erf()$ the error function, I the image intensity, $\beta_{l,u}$ the FWHM solutions, θ the slope of the error functions, ∇I the gradient magnitude and τ the threshold on the gradient magnitude. The FWHM-based component is the dominant factor for determining the exact boundaries due to the positive and negative range of the function preventing potential leaking usually occurring with strictly positive ranged functions only. The corresponding plot is similar to the plot of P_{fwhm} (Fig. 2) and is therefore omitted except for the difference in range for both functions: at the FWHM boundaries the function takes value zero instead of value 0.5. The addition of the (thresholded) gradient, which basically sets the pre-dominant FWHM term to zero above a user-defined given threshold, is useful to control the evolving contour in regions where lumen touches calcium tissues.

Because intensity in lumen contrast varies due to differences in contrast fluid concentration (especially along the vessel axis direction), we use a slice-based intensity term to have local control of the level set. The use of axial slices is justified by the fact that, owing to patient anatomy and the scanning protocol (Section 3), in most slices the carotid bifurcation is close to being perpendicular to the slice direction. Using the paths found in the previous step, we traverse along the path and calculate the mean and standard deviation in a small circular neighborhood as function of the axial slice, μ_l and σ_l, and the global mean and standard deviation for the complete path μ_g and σ_g. To construct the speed function F_{segm}, a new mean and standard deviation are defined by weighting the local and global values by a user-defined parameter η, i.e.

$$\mu' = (1-\eta)\cdot\mu_l + \eta\mu_g$$
$$\sigma' = (1-\eta)\cdot\sigma_l + \eta\sigma_g$$

Here we assume that both the local and global intensity distributions are sufficiently close which is a reasonable assumption considering the small extent of the local neighborhood. The stopping criterion is implemented by thresholding the root mean squared intensity difference with respect to the previous iteration. After convergence of the GAC, the segmentation is defined as the final level set image. In some experiments because small but consistent under-segmentation was observed, we introduce an additional variable which allows to locally expand the final segmentation with a distance parameter.

3. Study population

The study population was selected from a group of consecutive patients (November 2002–December 2005) with ischemic cerebrovascular disease, including amaurosis fugax (monocular visual loss), transient ischemic attack (TIA) or minor ischemic stroke (ranking score $\leqslant$3). Patients were enrolled from the specialized TIA/stroke out-patient clinic or neurology ward. During workup all patients underwent CTA of the carotid arteries. CTA was per-

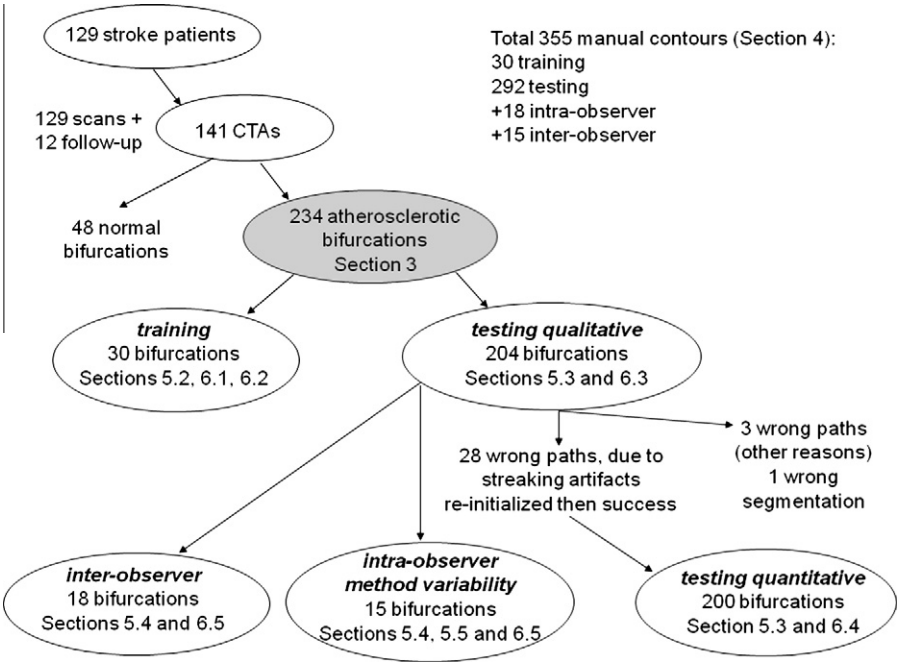

Fig. 4. Overview of the selected patients, bifurcations and conducted studies. Training of the method is carried out on a separate set of 30 bifurcations using the manual segmentation of one observer. In total, 204 atherosclerotic bifurcations were used for testing. After visual inspection of path tracking and lumen segmentation, 200 were included for the quantitative analysis.

formed within a research protocol which aims to assess the diagnostic accuracy of CTA in comparison to duplex ultrasound. The study was approved by the Institutional Review Board and all patients gave written informed consent.

The CTA data were acquired on a 16-row CT scanner (Sensation 16 – Siemens Medical Solutions, Forchheim, Germany) with a standard scan protocol using the following parameters: 120 kV, 180 mAs, collimation 16×0.75 mm, table feed per rotation 12 mm, pitch 1.0, rotation time 0.5 s and scan time 10–14 s. The CTA scan range is from the ascending aorta to the intracranial circulation (2 cm above the *sella turcica*). All patients received 80 ml contrast material (Iodixanol 320 mg/ml, Visipaque Amersham Health, Little Chalfont, UK), followed by a 40 ml saline bolus chaser; both had an injection rate of 4 ml/s. Synchronization between the passage of contrast material and data acquisition was achieved by real time bolus tracking at the level of the ascending aorta. The trigger threshold was set at an increase in attenuation of 75 Hounsfield Units (HU) above baseline attenuation (~150 HU in absolute HU value). Image reconstructions were made with a field-of-view 100 mm, matrix size 512×512 (real in-plane resolution 0.6×0.6 mm), slice thickness 1.0 mm, increment 0.6 mm and with an intermediate reconstruction algorithm (De Monyé et al., 2005, 2006; De Weert et al., 2008).

For the present study we selected patients with atherosclerotic disease in the carotid bifurcation, which was defined as the presence of calcifications and/or thickening of the vessel wall. A total of 234 bifurcations from 141 CTA scans were included, obtained from 129 stroke patients of which 12 patients were scanned twice for follow-up studies. The remaining 48 bifurcations had no atherosclerotic disease and were not taken into account in this study. Fig. 4 presents an overview of the patient data and selected bifurcations.

4. Expert segmentations

The reference standard for the evaluation of our method was obtained by four expert observers, each with 2–3 years of experience. To support the manual procedure of obtaining the reference standard, a custom made tool was developed in MeVisLab (MeVisLab) in close collaboration with the expert observers and experienced radiologists, for the drawing of contours to delineate the outer vessel wall, to separate calcium from lumen, and to sample the lumen intensity statistics. Within the outer vessel wall, lumen, calcium and plaque components were then segmented based on region growing and thresholding. A detailed description of the segmentation protocol has been reported (De Weert et al., 2008). A total of 355 manual contours were used: 30 for training, 292 for testing, 18 to assess the inter-observer variability, and 15 to assess the intra-observer variability. Detailed descriptions of these studies are given below and summarized in Fig. 4.

5. Experiments

5.1. Implementation and parameters

The method was implemented in ITK (Ibáñez et al., 2005) and a graphical user interface was made with MeVisLab (MeVisLab). Pilot experiments revealed which parameters could be set at fixed values, and which parameters required training. Fixed parameters were: the slope of the error function θ in P_{fwhm} (20), the neighborhood around the seed points for estimating the Gaussian μ and σ (2 voxel radius), the slope of the error function θ in F_{segm} (20), the stopping criterion (10^{-3} RMS), the number of iterations (1000), the neighborhood for estimating the intensity statistics along the path (4 voxel radius) and the scale at which the gradient magnitude is computed in F_{segm} (voxel size). After path tracking a region of interest was selected around the paths which was resampled to isotropic voxel sizes. The following parameters required training: the slope and threshold values of the error functions of the homogeneity filter $\theta_{v,g}$ and $\alpha_{v,g}$, the threshold of the gradient magnitude τ in F_{segm}, the post distance value ϕ to expand the final level set, the initial distance ρ of the GAC, the balance between local and global intensity statistics η, the weighting of the advection term α, and finally the weighting of the curvature term γ. The parameters for

path tracking were optimized separately from the parameters for segmentation. For practical reasons, all parameters were optimized individually in the order as listed above.

5.2. Training

We selected 30 carotid bifurcations of 18 patients for training, and an overlap measure is used as the evaluation criterion (Section 5.6). To achieve the best possible representation of the anatomical and pathological variability, these 30 bifurcations covered the range of possible degrees of stenosis: 13 carotids in category 0–29%, 7 in 30–49%, 5 in 50–69% and 5 in 70–99%. Degrees of stenosis were estimated visually. In addition, a sensitivity analysis of the method was carried out by varying the parameter settings by ±20% (with a step size of one percent) around the optimal values and observing their influence on the similarity index.

5.3. Testing

After training the method was applied to the remaining set of 204 carotid bifurcations, all of which were qualitatively evaluated for the correctness of path tracking and lumen segmentation. The qualitative evaluation was carried out by visual inspection to determine whether the paths were found within the branches of the bifurcation, and to determine whether the segmentation had not leaked into the background or vein structures. Segmentations of four expert observers were available to quantitatively evaluate the method on all data sets. In addition, the evaluation results were grouped by observer.

5.4. Observer variability

To assess the inter-observer variability, 18 carotid bifurcations were manually and independently analyzed by two observers. To assess the intra-observer variability of the expert segmentations 15 carotid bifurcations were segmented twice by one observer with a 4-month interval.

5.5. Method variability

To assess the method's variability (i.e. the dependency of segmentation results based on the placement of the seed points for initialization of the algorithm), we took the same set of bifurcations used to assess the intra-observer variability and replaced three times the initialization points for path tracking and subsequent segmentation.

5.6. Evaluation criteria

First, we visually inspected the extracted internal and external carotid artery paths and the lumen segmentation. Then, we determined the similarity index (SI) and the average surface distance between two segmentations to evaluate the accuracy of the segmentation quantitatively. Because the manually obtained lumen segmentations were usually confined to a small region of interest around the bifurcation, often containing only the common and internal arteries (sometimes to the external artery if pathology is present) the evaluation was limited to this part. The similarity index, or Dice coefficient, is a normalized overlap measure:

$$SI = \frac{2|A \cap B|}{|A| + |B|}$$

Here $|.|$ denotes the cardinality operator and $\cap$ the intersection. Besides the SI of the lumen-method and lumen-observer, we also report the SI of the lumen-method and calcium-observer and the SI of the lumen-method and the soft plaque-observer components separately, to determine how much calcium and soft plaque was wrongly classified as lumen. By soft plaque we mean fiber tissue and lipids. The average surface distance is approximated by calculating the error volume (misclassified voxels) divided by the surface area of the manual segmentation, where the surface area is approximated by the average of an erosion and a dilation of the segmentation, i.e.

$$\bar{d} = \frac{\sim vol_{error}}{\sim area_{surface}} = \frac{h^3 \cdot |X(A,B)|}{h^2 \cdot 1/2 \cdot |(B - \varepsilon(B)) + (\partial(B) - B)|}$$

Here h denotes voxel size, X is the exclusive OR operator, A the result of the method, B the result of manual segmentation, $\varepsilon()$, $\delta()$ the morphological erosion operator and dilation operator with circular structuring element of size h.

6. Results

6.1. Training: path tracking

To determine the threshold values α_v and α_g of P_{std}, plots of the training set were generated as shown in Fig. 3. This revealed that the optimal threshold setting was 10 and 20 HU, respectively, which is confirmed by inspection of the light and dark blue lines in the representative example shown in Fig. 2. The best parameter for the slope of the error functions $\theta_{v,g}$ was found by searching in the range 5–50 HU with steps of 5 HU; for both parameters the best setting was 20 HU. These optimal settings showed that in one bifurcation of the training set the correct (internal) path could not be found due to the similar intensity of the veins touching the carotid artery.

6.2. Training: segmentation

The threshold of the image gradient τ in F_{segm} was optimized first between values $[100 \ldots 200]$. Besides the similarity index we also visually inspect the results since this parameter setting influences possible leaking of the segmentation into veins or calcified regions. A final setting of 107 yielded the best results. The post distance ϕ had optimization range $[0.0 \ldots 1.0]$, balance η had $[0.0 \ldots 1.0]$, initial distance ρ $[0.1 \ldots 1.5]$, advection α $[0, 10^{-4}, 10^{-3}, 10^{-2}]$ and curvature γ $[0, 10^{-4}, 10^{-3}, \ldots 1.0]$. The final settings were $\phi = 0.6$, $\eta = 0.3$, $\rho = 0.5$, $\alpha = 10^{-2}$ and $\gamma = 10^{-4}$, respectively. The results of the sensitivity analysis are shown in Fig. 5. The optimal setting is at zero percent and around this setting the similarity index remains above 0.89.

6.3. Testing: qualitative evaluation

Table 1 summarizes the qualitative evaluation for training and testing. In the first run of the test set with seed points placed as shown in Fig. 1, 31 out of 204 paths were erroneously tracked in the sense that some parts of the path are outside the arterial lumen. All these errors were caused by severe streaking artifacts, located above the bifurcation and due to dental implants.

For those bifurcations we replaced the internal and external seed points proximal to the region containing the streaking artifacts, while still including the atherosclerotic part of the carotid artery. After re-initialization, three erroneous paths remained: Case one contained a severe stenotic internal artery, such that no remaining lumen can be observed causing the minimum cost path to jump into another nearby artery. Case two contained very low contrast distal to the bifurcation. Case three contained a neighboring high contrast artery distal to the bifurcation, resulting in an erroneous jump of the minimum cost path. Apart from these three

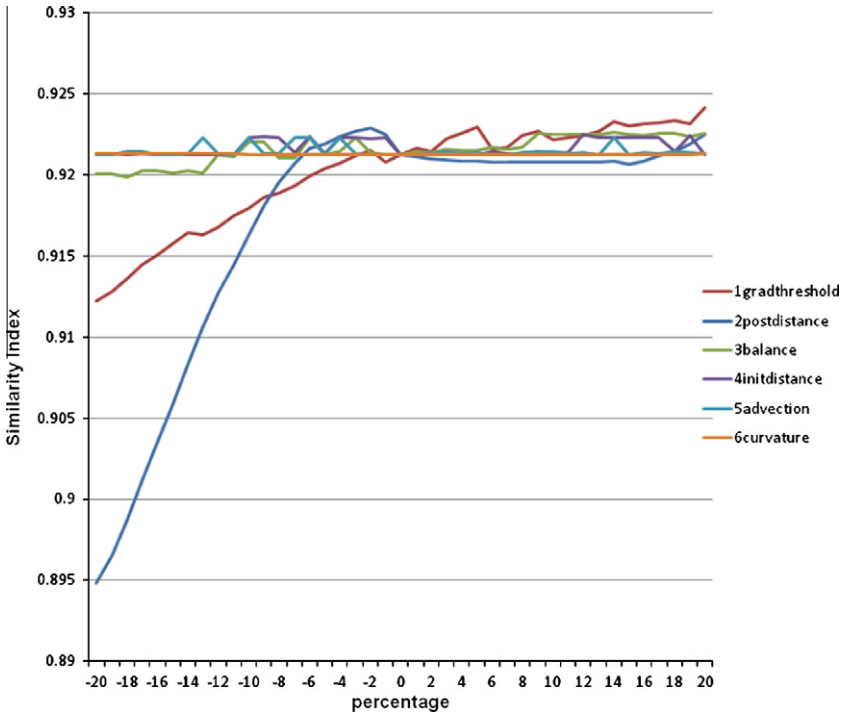

Fig. 5. The influence on the similarity index if the parameter settings are changed around the optimal settings at zero percent. For ±20% variation, the similarity index remains above 0.89.

Table 1
Qualitative evaluation of the method, assessing the correctness of the prior path tracking and final lumen segmentation on the training set and the remaining set of bifurcations.

	Number of bifurcations	Correctly extracted paths	Correctly extracted lumen
Training	30	29	29
Remaining	204	201 (99%)	200 (98%)
	234		

tracking errors, only one lumen segmentation was unsuccessful (Fig. 6), caused by the neighboring jugular vein having an intensity value similar to the arterial lumen; this is probably due to non-optimal timing of scanning with respect to arrival of the contrast bolus.

Fig. 7 shows some representative examples of the performance of the method in case of the presence of calcified and non-calcified (soft) plaque and stenosis. On visual inspection, the calcified bifurcations were correctly segmented; in case of severe stenosis the method resulted in a slight under-segmentation of the lumen. Finally, some 3D renderings of the segmentation results are shown in Fig. 8.

6.4. Testing: quantitative evaluation

In the 200 carotid bifurcations with a correctly segmented lumen, 292 expert segmentations were available for comparison.

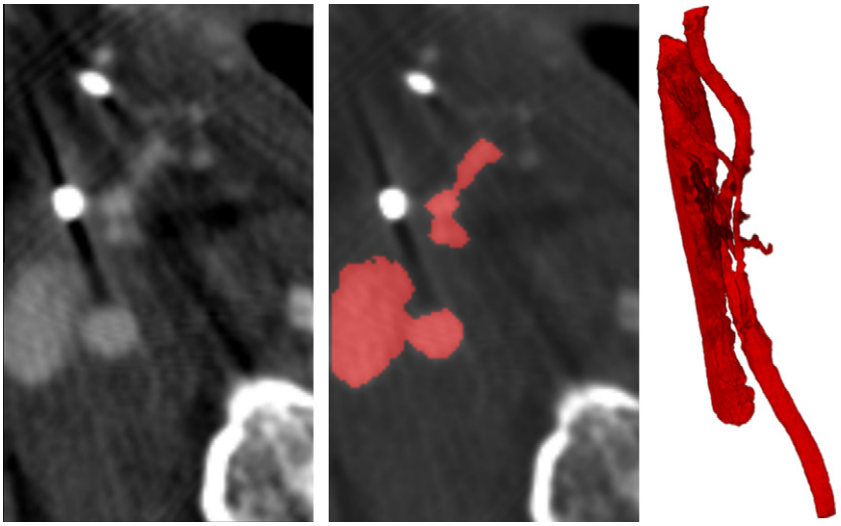

Fig. 6. The only wrong segmentation from the test set. The left and middle images are axial slices in which the segmentation erroneously jumped from an artery to the jugular vein which had an intensity similar to the arterial lumen. The right image is a 3D volume rendering of the final segmentation result.

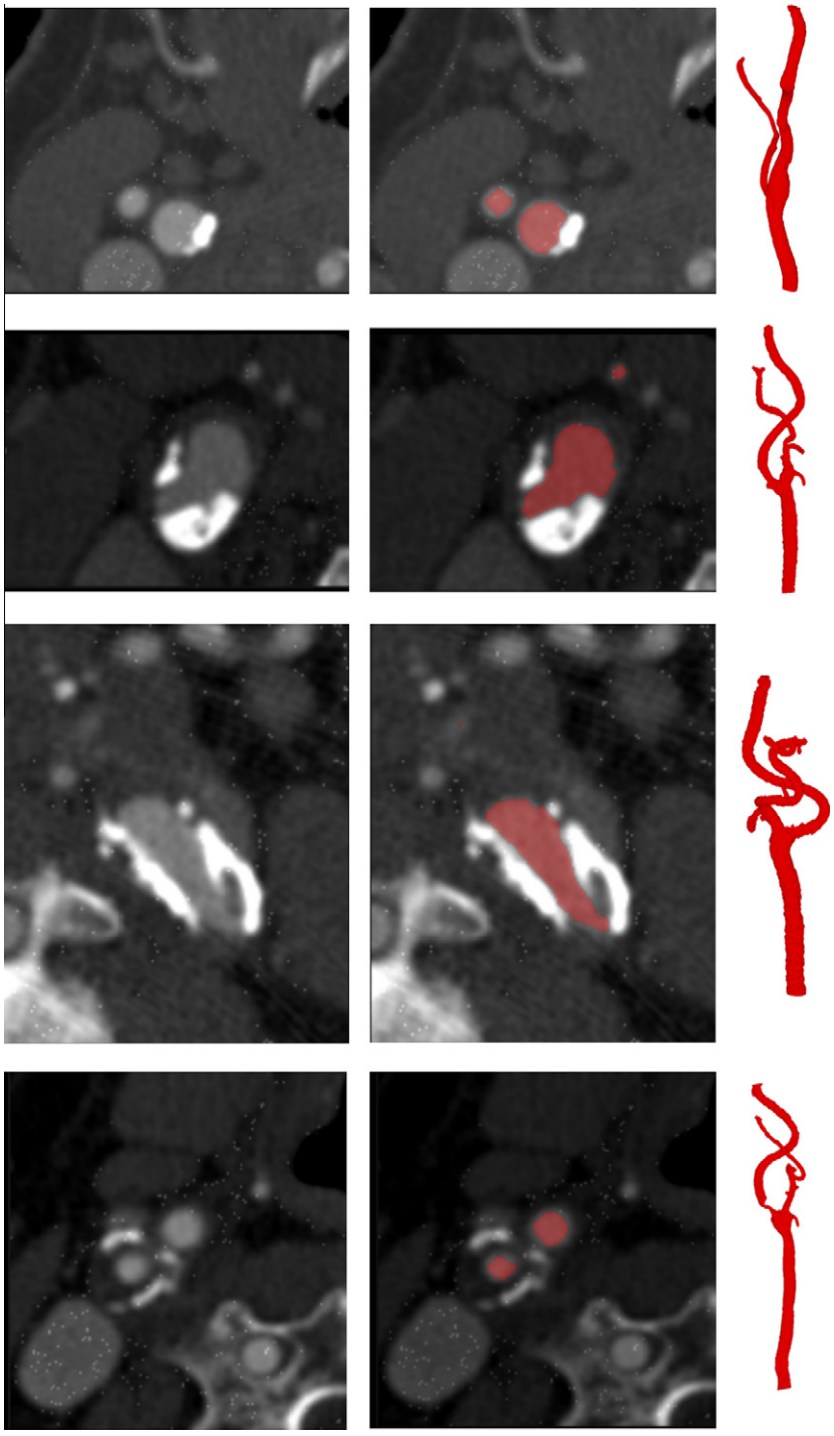

Fig. 7. Representative examples of the segmentation results obtained by our method in case of the presence of severe calcified and non-calcified (soft) plaque (rows 1–3) and stenosis (bottom row).

The erroneously tracked paths and wrong lumen segmentation were removed before the quantitative evaluation. Table 2 gives the results of the quantitative evaluation, and Table 3 the quantitative results grouped per observer. The following observations can be made: the quantitative results (Table 2) show that the SI of the training set is lower than that for the evaluation studies, suggesting that an appropriate training set was selected. Grouping the quantitative results by individual observers (Table 3) indicates that, although the method was trained on contours of only one observer (O2), this had little influence on the results compared to the other observers (O1, O3 and O4).

6.5. Observer and method variability

Table 4 gives the results on the assessment of the variability between the observer's and the methods'. Note that for the SI measurements we always compare the results of lumen versus the other components; for example, the third row shows the overlap

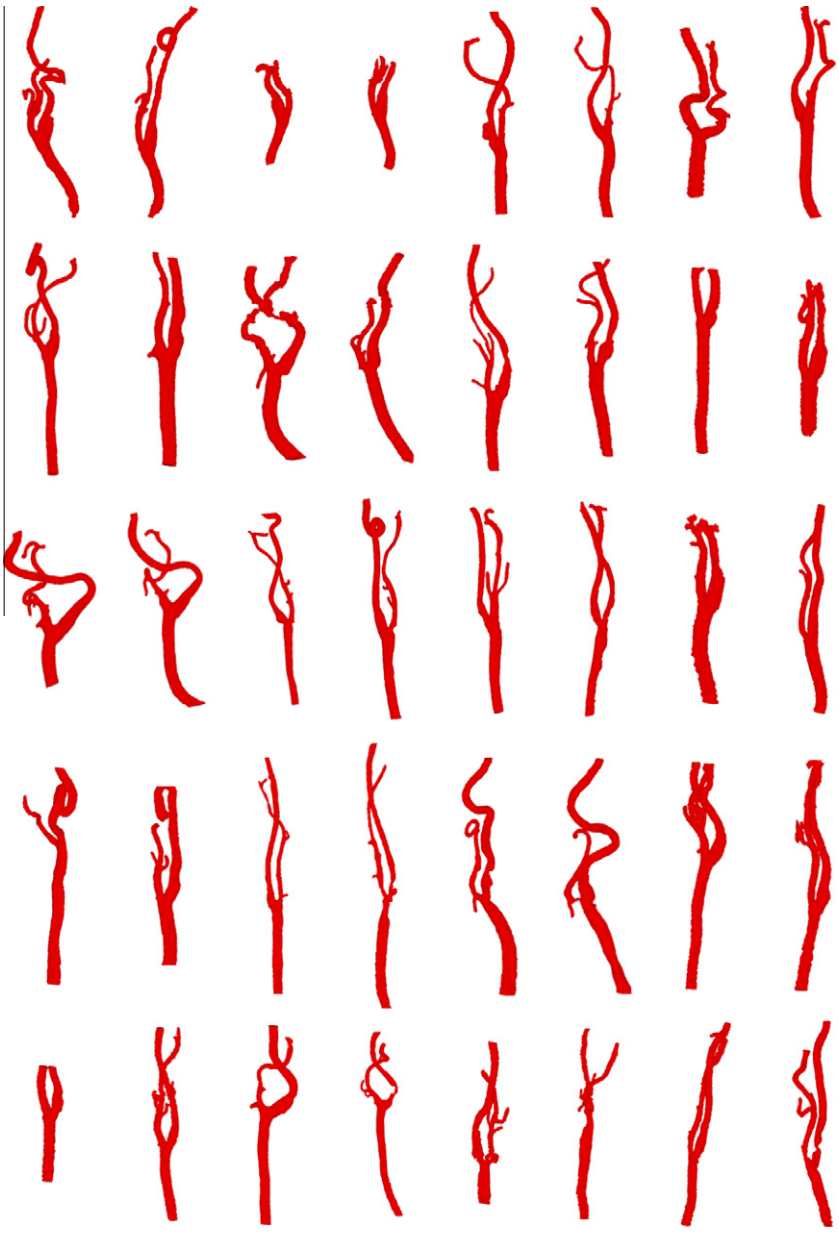

Fig. 8. Volume renderings of the first 40 lumen segmentations of the carotid bifurcation from the test set.

Table 2
Quantitative evaluation of the method by comparison with the manually annotated lumen. Soft plaque refers to non-calcified plaque and includes tissue, fiber tissue and lipids.

Study	Manual segmentations	Bif.	SI lumen	SI calcium	SI soft plaque	Distance lumen (mm) mean ± std min–max
Training	29	29	0.92	0.03	0.06	0.13 ± 0.07 0.07–0.32
Testing	292	200	0.94	0.05	0.03	0.11 ± 0.07 0.04–0.90

Table 3
Quantitative results of the testing study grouped per observer.

	Manual segmentations	SI lumen	Distance lumen (mm) mean ± std min–max
O1	6	0.95	0.09 ± 0.02 0.06–0.13
O2	113	0.93	0.11 ± 0.08 0.06–0.90
O3	18	0.94	0.11 ± 0.05 0.06–0.24
O4	155	0.94	0.11 ± 0.04 0.04–0.82
	292		

measurements of the lumen segmented by observer 1, compared to lumen, calcium and soft plaque (columns 4–6) of observer 2. The following observations can be made: the SI between the method and manual segmentations is similar to that of the inter-observer (0.92 vs. 0.87) and the intra-observer (0.94 vs. 0.94). The errors in terms of overlap with non-lumen components are similar as well (columns 5 and 6 for both the inter-observer as the intra-observer comparisons), suggesting that the automated method has the potential to replace the manual procedure. The dependency of the method on seed points initialization is relatively low, which

Table 4
Results on the variability between the observer's and methods'.

	Manual segmentations	Bif.	SI lumen	SI calcium	SI soft plaque	Distance lumen (mm) mean ± std min–max
Inter-observer						
Method – Obs1	18	18	0.92	0.04	0.02	0.13 ± 0.03 0.08–0.18
Method – Obs2	18	18	0.92	0.06	0.02	0.13 ± 0.03 0.08–0.18
$Obs1_{lumen}$–Obs2	17	17	0.87	0.03	0.01	0.28 ± 0.21 0.02–0.91
Intra-observer						
Method – ObsT1	15	15	0.94	0.03	0.04	0.10 ± 0.02 0.06–0.14
Method – ObsT2	15	15	0.94	0.04	0.04	0.10 ± 0.02 0.06–0.14
$ObsT1_{lumen}$–ObsT2	15	15	0.94	0.03	0.01	0.11 ± 0.10 0.01–0.40
Method variability						
Three seed points sets, average	15	15	0.97	–	–	0.05 ± 0.04 0.00–0.16

is reflected in a high average SI (0.97) between the method results and the manual contours of the intra-observer set.

7. Discussion

We have proposed and evaluated a semi-automatic method for lumen segmentation of the carotid bifurcation in CTA. The only user interaction required is the manual initialization of the method by clicking three points, i.e. in the common artery and the internal and external carotid arteries. Then, two paths are tracked using inhomogeneity and intensity information. Finally, a level set-based lumen segmentation steered by a balanced intensity and gradient-based speed function of the vessel lumen is achieved. The combination of path tracking and segmentation has proven valuable in vessel segmentation (Aylward and Bullit, 2002; Van Bemmel et al., 2003b). In the present study the path is used for initialization and for defining a speed function based on local intensity information.

The main contribution of this work is the evaluation of our method in a large number of patients with atherosclerotic disease in the carotid bifurcation, i.e. the presence of calcified and non-calcified plaque and/or lumen narrowing. We think that the included atherosclerotic bifurcations represent of the variability in pathology and image quality present in clinical practice. Path tracking failed in only 3 of the 204 cases (due to severe stenosis, severe calcifications, and remaining streaking artifacts). Only one lumen segmentation included parts of the vein (due to the jugular vein having a similar intensity). Comparison with manual segmentations showed that the method performs similar to the observers in terms of overlap measures. Visual inspection of severely calcified bifurcations revealed that the method performs satisfactorily, in the sense that the lumen segmentation can be used for subsequent analysis (e.g. plaque detection and quantification, and hemodynamic analysis). Severely stenotic bifurcations resulted in a slight under-segmentation of the lumen probably caused by the dominating effect of partial volume voxels.

In the present study, albeit bifurcations for training were carefully selected to include varying degrees of stenosis, it is encouraging that developing and training of the method can be performed on a relatively small number of patients and using manual segmentations from only one observer.

This work also has some limitations, the main one being the failure of path tracking in CTA data-sets containing streaking artifacts. This concerned 28 cases, but could easily be overcome by replacing the initialization points below this region. Setting seed points proximal of streaking artifacts has no influence on the clinical usefulness of the method, as the diseased part of the vessel was still contained in the segmentation. Another limitation is under-segmentation in the case of severely stenotic bifurcations; this should be taken into account if subsequent automatic stenosis analysis is performed based on this method. Finally, the need for the user to click points in branches of the bifurcations is considered a limitation. Pilot studies revealed that this interaction was still required to guarantee a practical level of robustness of the method. Although point clicking can be carried out easily and quickly, it remains an undesirable interruption of the clinical workflow. However, we are currently investigating robust approaches for fully-automated segmentation of the atherosclerotic carotid bifurcation in CTA.

Acknowledgments

This research was supported by Economic Affairs innovation grant IS044070 Automatic Diagnostic Vascular Analysis of CTA Examinations (ADVANCE). Aad van der Lugt is recipient of a fellowship from the Netherlands Organization for Health Research and Development (NWO-KF Grant No. 907-00-122). The authors are grateful to Marjon van Gils and Harald Groen (Erasmus Medical Center Rotterdam) for their use, interest and feedback on the (preliminary) segmentation results during the development of the segmentation method.

References

Antiga, L., Ene-Iordache, B., Caverni, L., Cornalba, G., Remuzzi, A., 2002. Geometric reconstruction for computational mesh generation of arterial bifurcations from CT angiography. Comput Med Imaging Graph 26 (4), 227–235.

Aylward, S.R., Bullit, E., 2002. Initialization, noise, singularities, and scale in height ridge traversal for tubular object centerline extraction. IEEE Transactions on Medical Imaging 21 (2), 61–75.

Boykov, Y.Y., Jolly, M.P., 2001. Interactive graph cuts for optimal boundary and region segmentation of objects in *n*-D images. In: Proceedings of the Eighth IEEE International Conference on Computer Vision (ICCV), vol. 1, pp. 105–112.

Caselles, V., Kimmel, R., Sapiro, G., 1997. Geodesic active contours. International Journal of Computer Vision 22 (1), 61–79.

Chan, T.F., Vese, L.A., 2001. Active contours without edges. IEEE Transactions on Image Processing 10 (2), 266–277.

De Monyé, C., Cademartiri, F., De Weert, T.T., Siepman, D.A.M., Dippel, D.W.J., Van der Lugt, A., 2005. Sixteen-detector row CT angiography of carotid ateries: comparison of different volumes of contrast material with and without a bolus chaser. Radiology 237 (2), 555–562.

De Monyé, C., De Weert, T.T., Zaalberg, W., Cademartiri, F., Siepman, D.A.M., Dippel, D.W.J., Van der Lugt, A., 2006. Optimization of CT angiography of the carotid artery with a 16-MDCT scanner: craniocaudal scan direction reduces contrast material-related perivenous artifacts. American Journal of Roentgenology 186 (6), 1737–1745.

De Weert, T.T., De Monyé, C., Meijering, E., Booij, R., Niessen, W.J., Dippel, D.W.J., Van der Lugt, A., 2008. Assessment of atherosclerotic carotid plaque volume with multidetector computed tomography angiography. International Journal of Cardiovascular Imaging 24 (7), 751–759.

Dijkstra, E.W., 1959. A note on two problems in connexion with graphs. Numerische Mathematic 1, 269–271.

Florin, C., Paragios, N., Williams, J., 2005. Particle filters, a quasi-Monte-Carlo-solution for segmentation of coronaries. In Medical Image Computing and Computer Assisted Intervention (MICCAI) 8, 246–253.

Homann, H., Vesom, G., Noble, J.A., 2008. Vasculature segmentation of CT liver images using graph cuts and graph-based analysis. In: Proceedings of the 5th

IEEE International Symposium on Biomedical Imaging (ISBI): From Nano to Macro, pp. 53–56.
Hoogeveen, R.M., Bakker, C.J.G.L., Viergever, M.A., 1998. Limits to the accuracy of vessel diameter measurements in MR angiography. Journal of Magnetic Resonance Imaging 8 (6), 1228–1235.
Ibáñez, L., Schroeder, W., Ng, L., Cates, J., 2005. The ITK Software Guide, second ed. Kitware, Inc.
Lorigo, L.M., Faugeras, O.D., Grimson, W.E.L., Keriven, R., Kikinis, R., Nabavi, A., Westin, C.-F., 2001. CURVES: curve evolution for vessel segmentation. Medical Image Analysis 5 (3), 195–206.
MeVisLab. Software for medical image processing and visualization. <http://www.mevislab.de>.
Mildenberger, P., Kauczor, H.U., Ehrhard, K., Schmiedt, W., Thelen, M., 1997. CT-angiography in carotid stenosis. Radiology 37 (11), 883–890.
Rozie, S., De Weert, T.T., De Monyé, C., Homburg, P.J., Tanghe, H.L.J., Dippel, D.W.J., Van der Lugt, A., 2009. Atherosclerotic plaque volume and composition in symptomatic carotid arteries assessed with multidetector CT angiography; relationship with severity of stensosis and cardiovascular risk factors. European Radiology 19 (9), 2294–2301.
Schaap, M., Neefjes, L., Metz, C.T., Van der Giessen, A.G., Weustink, A.C., Mollet, N.R.A., Wentzel, J.J., Van Walsum, T., Niessen, W.J., 2009. Coronary lumen segmentation using graph cuts and robust kernel regression. In: Information Processing in Medical Imaging, vol. 5636. Lecture Notes in Computer Science, pp. 528–539.
Scherl, H., Hornegger, J., Prümmer, M., Lell, M., 2007. Semi-automatic levelset based segmentation and stenosis quantification of the internal carotid artery in 3D CTA data sets. Medical Image Analysis 11 (1), 21–34.
Sethian, J.A., 1999. Level Set Methods and Fast Marching Methods, second ed. Cambridge University Press.
Tarjàn, Z., Pozzi Mucelli, F., Frezza, F., Pozzi Mucelli, R., 1996. Three-dimensional reconstructions of carotid bifurcation from CT images: evaluation of different rendering methods. European Radiology 6 (3), 326–333.
Van Bemmel, C.M., Spreeuwers, L.J., Viergever, M.A., Niessen, W.J., 2003a. Levelset based artery–vein separation in blood pool agent CE-MR angiograms. IEEE Transaction on Medical Imaging 22 (10), 1224–1234.
Van Bemmel, C.M., Viergever, M.A., Niessen, W.J., 2003b. Semi-automated segmentation and stenosis quantification of 3D contrast-enhanced MR angiograms of the internal carotid artery. Magnetic Resonance in Medicine 51 (4), 753–760.
Vukadinovic, D., Van Walsum, T., Manniesing, R., Rozie, S., Hameeteman, R., De Weert, T.T., Van der Lugt, A., Niessen, W.J., 2010. Segmentation of the outer vessel wall of the common carotid artery in CTA. IEEE Transaction on Medical Imaging 29 (1), 65–76.
Yan, P., Kassim, A.A., 2006. Segmentation of volumetric MRA images by using capillary active contour. Medical Image Analysis 10 (3), 317–329.
Zhuge, F., Rubin, G.R., Sun, S., Napel, S., 2006. An abdominal aortic aneurysm segmentation method: level set with region and statistical information. Medical Physics 33 (5), 1440–1453.